CHAPTER V

VALIDATION OF CFD RESULTS

In this chapter, the CFD results of the R141b ejector model were validated with the experimental data. The boundary conditions of the simulated model were set as was done in the experiment. The primary fluid inlet conditions of the model were set to the saturated conditions corresponding to the vapour-generator temperature ranges from 90°C to 120°C. While, the secondary fluid inlet conditions were set to the saturated conditions corresponding to the evaporator temperature ranges from 0°C to 10°C. The downstream conditions of the ejector were varied from 0.7 bar to 1.8 bar corresponding to the condenser temperatures of around 25°C to 50°C. The validation process was performed by validating the CFD results of primary fluid mass flow rates, the entrainment ratios and the wall static pressure distributions of the R141b ejector model with the actual values.

5.1 Validation of the Primary Fluid Mass Flow Rate

Table 5.1 and Figure 5.1 compare the predictions of the primary fluid's flow rates through the primary nozzles by CFD with the experimental results when the primary fluid temperature was ranged from 90°C to 120°C. The primary flow rates predicted by CFD for both nozzles' throat diameter of 2.8 and 2.5 mm. were mostly over predicted compared to the measurement values. The average error of only 1.86 % was found for the predicted mass flow rate through the 2.8 mm. nozzle throat diameter; whereas a higher average error of only 5% was found for the nozzle whose throat diameter was 2.5 mm. This validation of

the primary mass flow rate, hence, guarantees the accuracy of the results of the flow through the primary nozzle.

Table 5.1 Validation of calculated primary mass flow rate with the experimental values.

	Primary mass flow rate, $\dot{m}_p$ (kg/s)					
T_P (°C)	Nozzle throat diameter= 2.8 mm			Nozzle throat diameter= 2.5 mm		
	CFD	Experiment	Error (%)	CFD	Experiment	Error (%)
90	0.0130	0.0129	0.9302	0.0103	0.0107	-3.8380
95	0.0145	0.0145	0.0144	0.0116	0.0113	2.3200
100	0.0162	0.0160	0.8739	0.0128	0.0123	4.7209
105	0.0179	0.0174	2.6965	0.0142	0.0133	6.6213
110	0.0198	0.0192	3.0729	0.0157	0.0147	7.1042
115	0.0218	0.0211	3.3175	0.0173	0.0159	8.8523
120	0.0240	0.0235	2.1277	0.0190	0.0177	7.6785
Average Error (%)			1.862			4.780

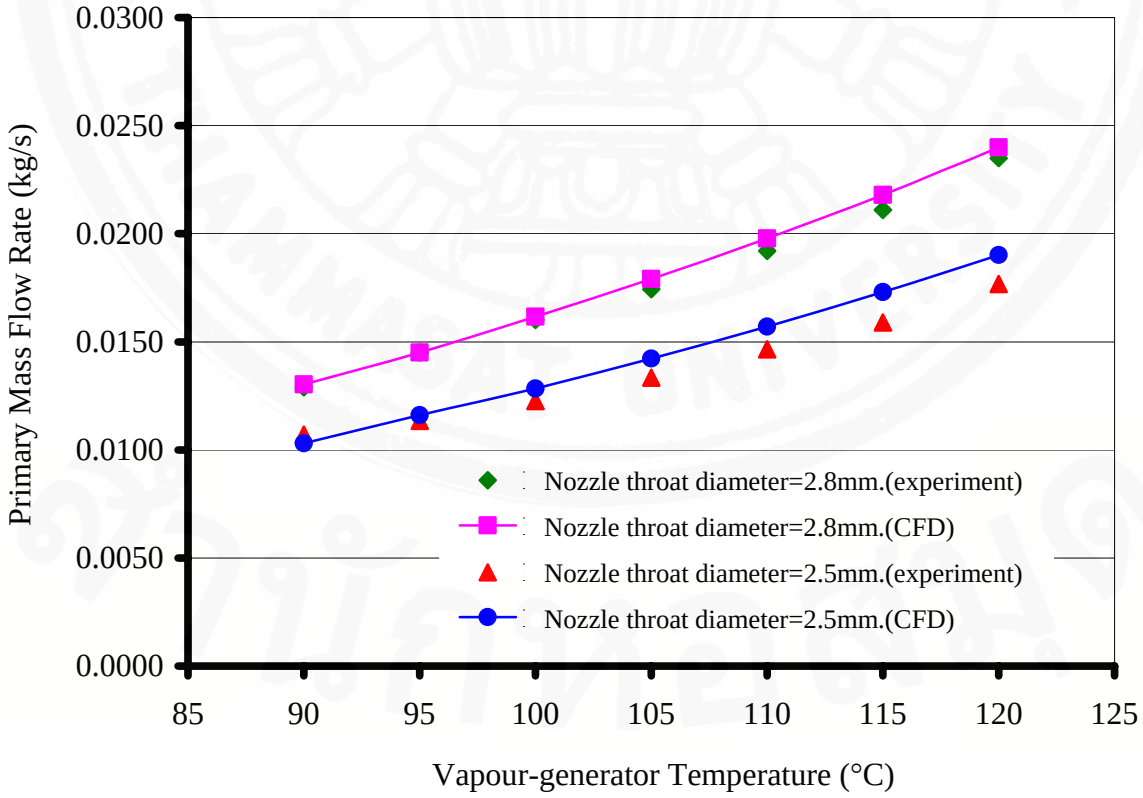

Figure 5.1 Comparison between CFD and experimental results of the primary mass flow rate.

5.2 Validation of the Wall Static Pressure Distributions

This section presents the validation of the calculated wall static pressure distributions with the experimental values. As described in Chapter III, the static pressures along the wall of the ejector were measured using the 8-port pressure manifold connected to an absolute pressure transducer (0-2.0 bar absolute). Each port of the pressure manifold was connected to the tapping hole drilled at the wall of the ejector, using polyethylene tube with 4mm. outer diameter. The measured static pressure distributions along the wall of the experimental R141b ejector were used as the reference data for validating with one from the simulated solutions.

Figure 5.2 to 5.7 illustrate the comparison between the static pressure distributions at the wall from the two different approaches, the experimental versus the simulated results. The comparisons of the calculated and the measured wall static pressure distribution at various downstream and upstream operating conditions are presented in Figure 5.2 and Figure 5.3, respectively. Also, the comparisons when the ejector was operated at various geometries are presented in Figure 5.4 to Figure 5.7.

The distributions of the predicted static pressure at the wall in Figure 5.2 to Figure 5.7 were mostly found to be offset lower than the one from the experiments, especially at the throat section. One possible reason for this error may come from the difficulty of calibrating the absolute pressure transducer at very low range near the absolute zero level. Another possible cause was thought to occur by an unexpected surface-roughness or mis-alignment in the primary nozzle and the ejector.

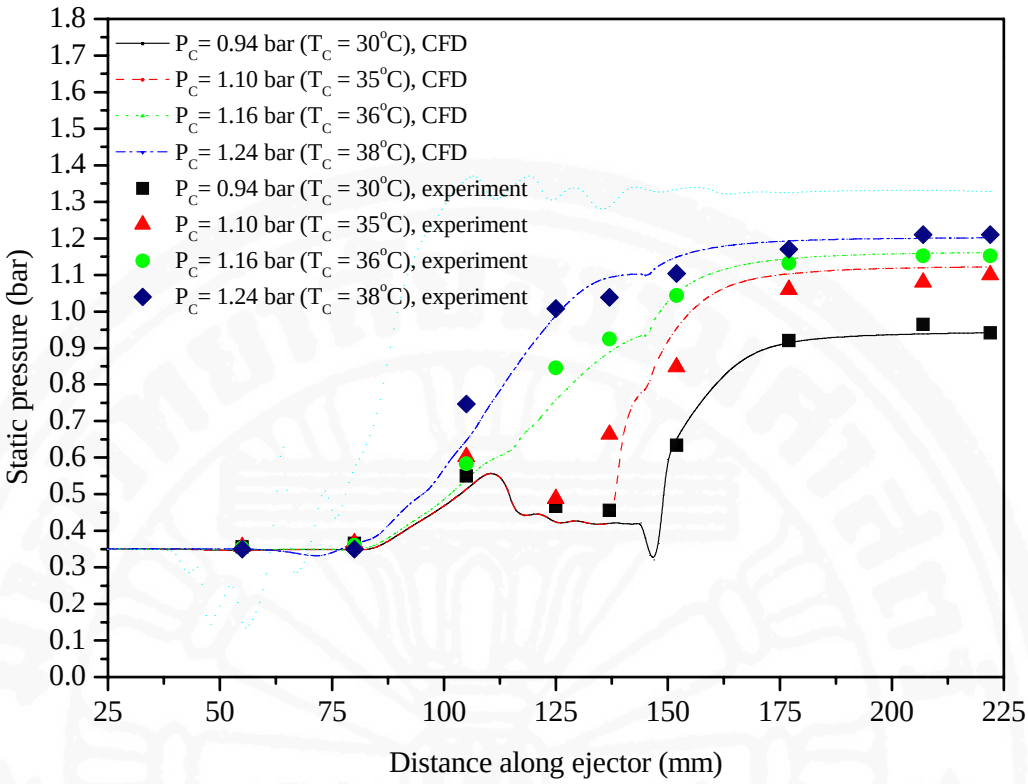

Figure 5.2 Static pressure profile along the ejector at T_P = 100°C, T_S = 5°C and at various condenser pressures, effect of downstream pressure.

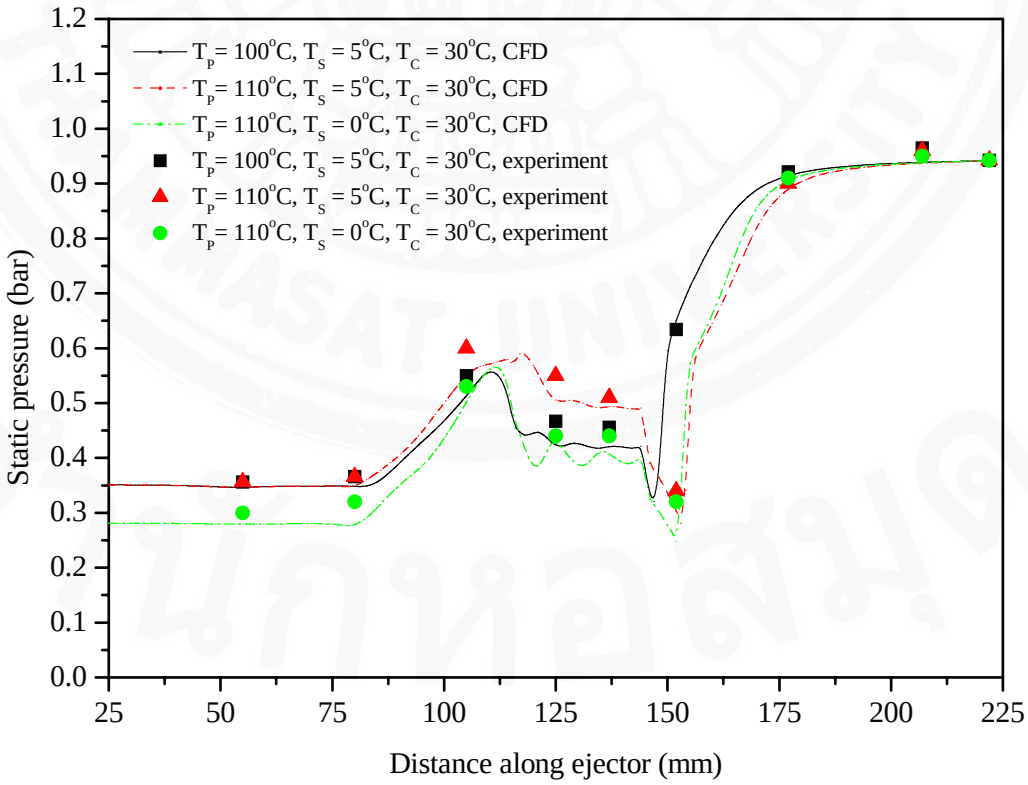

Figure 5.3 Static pressure profile along the ejector at T_C =30°C (P_C =0.94 bar), effect of primary and secondary fluid pressure.

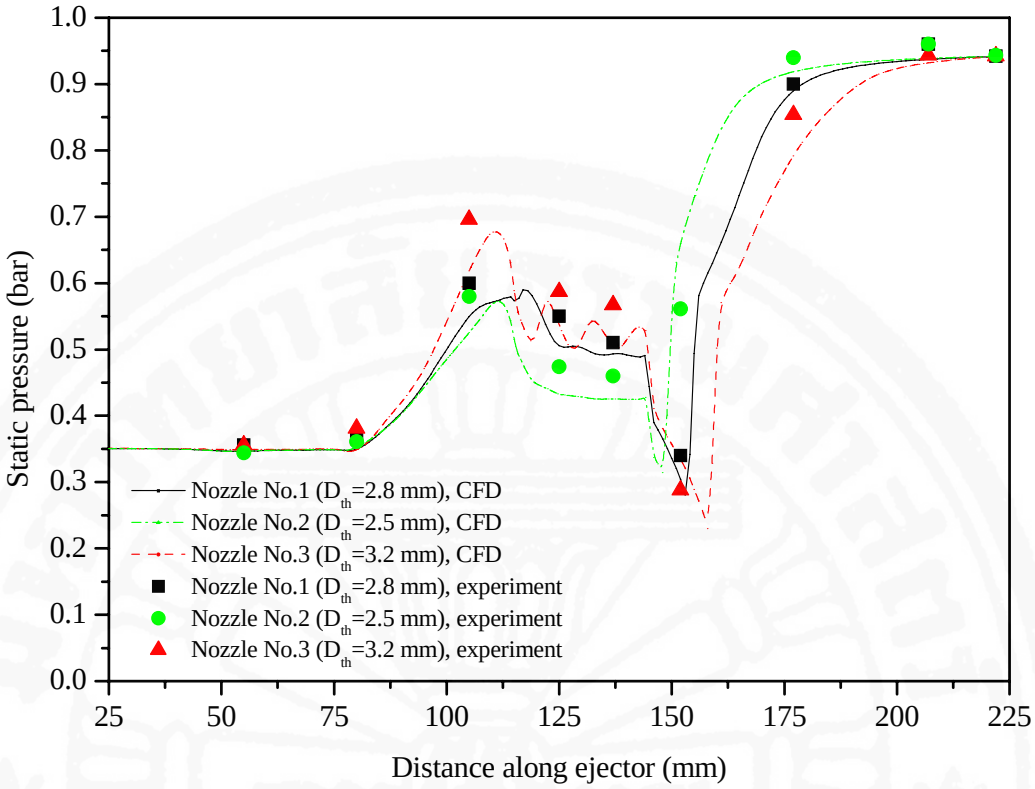

Figure 5.4 Static pressure profile along the ejector at T_P = 110°C, T_S = 5°C , and
P_C = 0.94 bar, effect of the primary nozzle throat diameter.

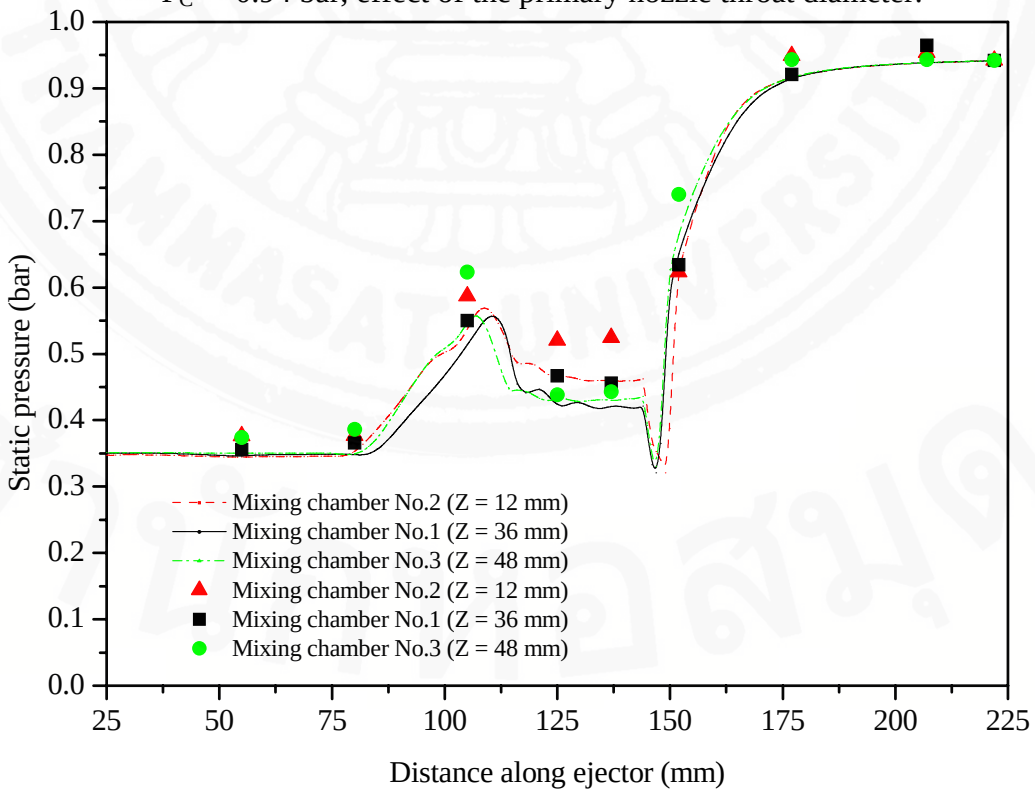

Figure 5.5 Static pressure profile along the ejector at T_P = 100°C, T_S = 5°C, and P_C = 0.94 bar, effect of the mixing chamber inlet diameter.

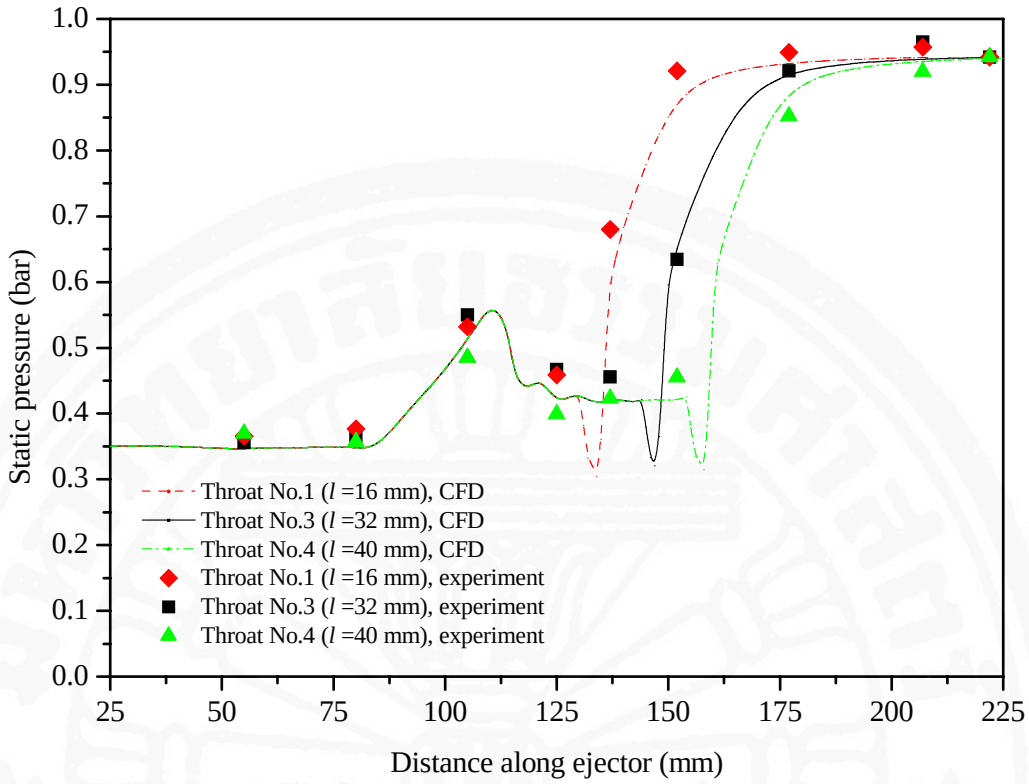

Figure 5.6 Static pressure profile along the ejector at T_P = 100°C, T_S = 5°C, and P_C = 0.94 bar, effect of the throat length.

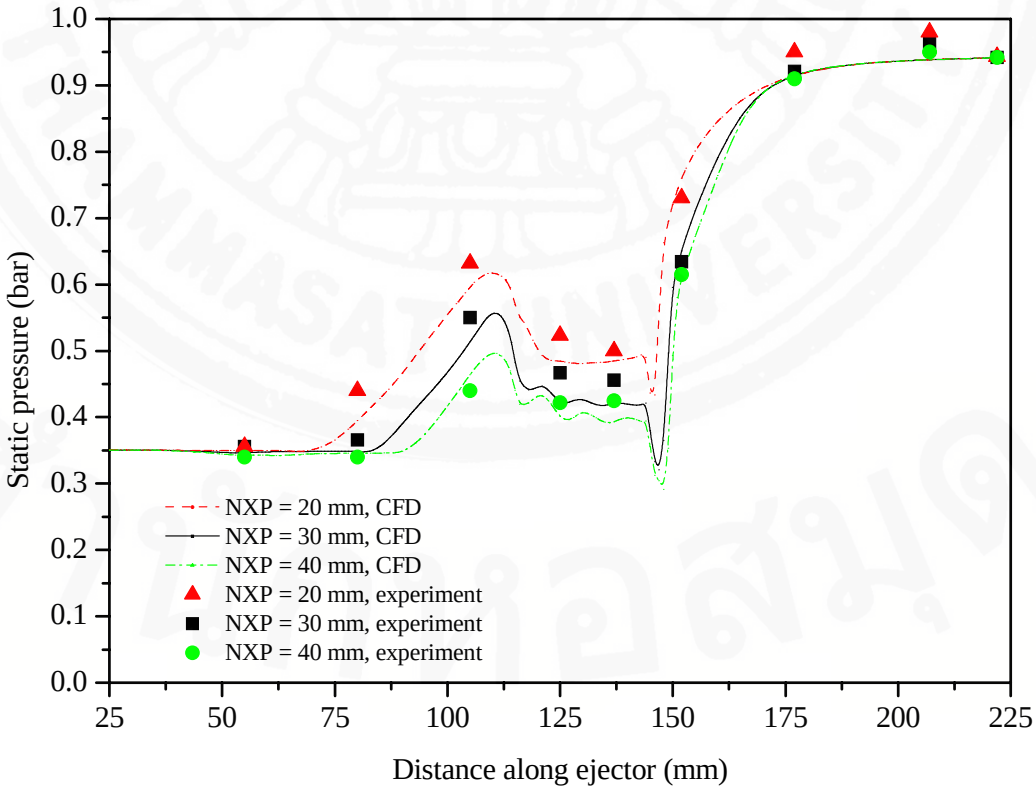

Figure 5.7 Validation of Static pressure profile along the ejector at T_P = 100°C, T_S = 5°C, and P_C = 0.94 bar, effect of the nozzle exit position (NXP).

5.3 Validation of the Entrainment Ratio and Critical Back Pressure

Regarding the calculated entrainment ratio, it was found to have good agreement with the results obtained from the experiments. Figure 5.8 and Table B.1 in Appendix B shows the similarity in the ejector performance characteristic between the calculated and the actual values, when the upstream and downstream operating conditions of the R141b ejector were varied. It is obvious that the predicted entrainment ratios are offset slightly lower than those of the experimental values. This error may come from the fact that the predicted values of the primary mass flow rates were found at higher rates compared to the actual values as discussed previously in section 5.1. Figures 5.9 to 5.12 also show the similarities in the ejector performance characteristic, when the ejector's operating geometries were varied, from the two different approaches, the experiment and the CFD method.

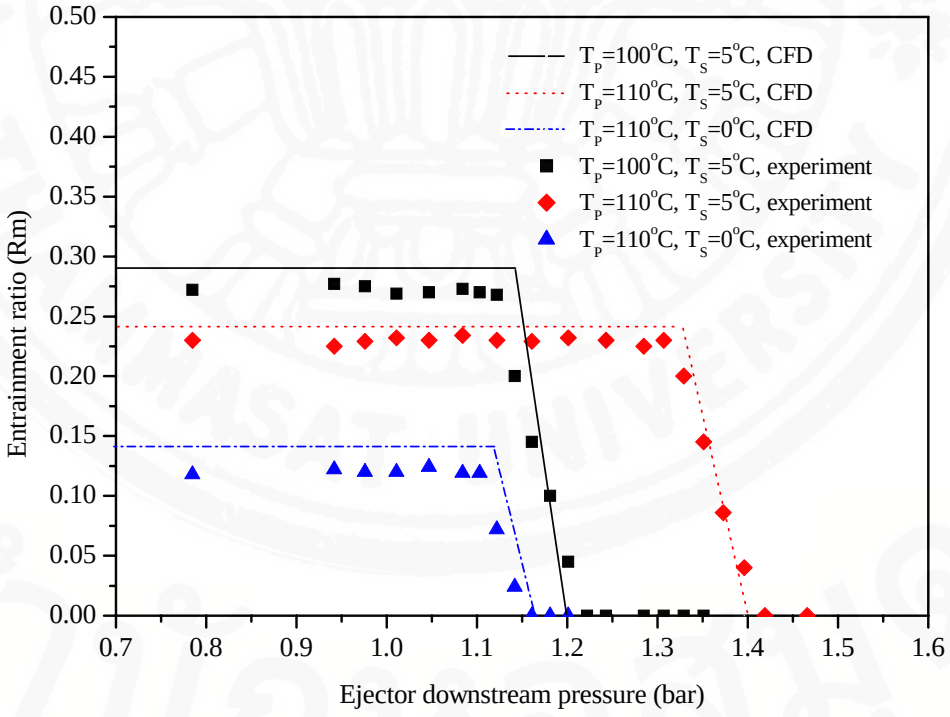

Figure 5.8 Validation of entrainment ratio, effect of operating conditions.

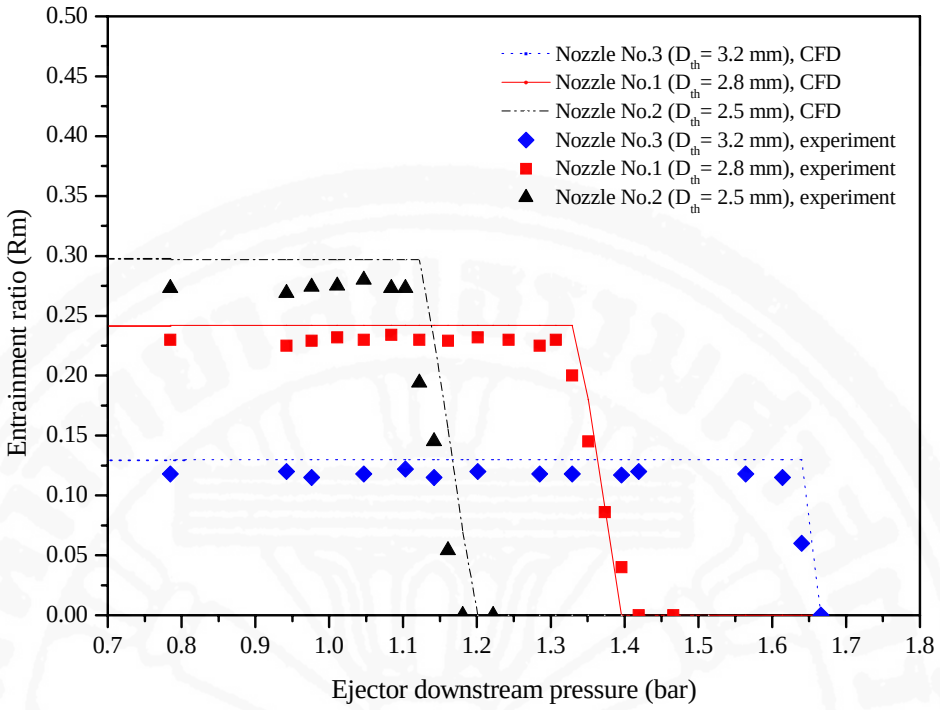

Figure 5.9 Validation of entrainment ratio, effect of primary nozzle throat diameter.

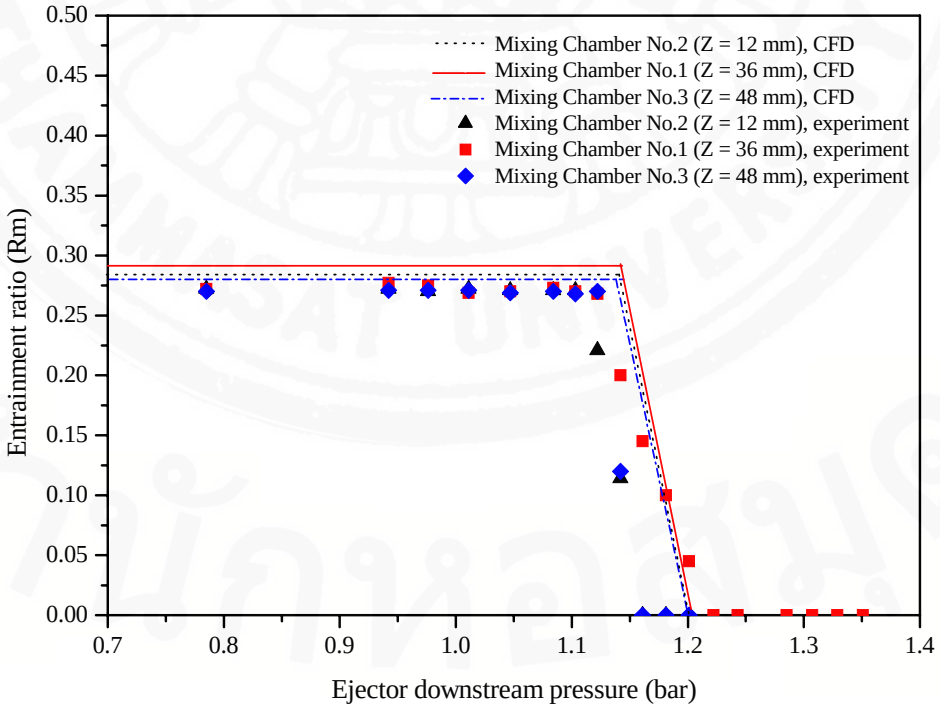

Figure 5.10 Validation of entrainment ratio, effect of mixing chamber inlet diameter.

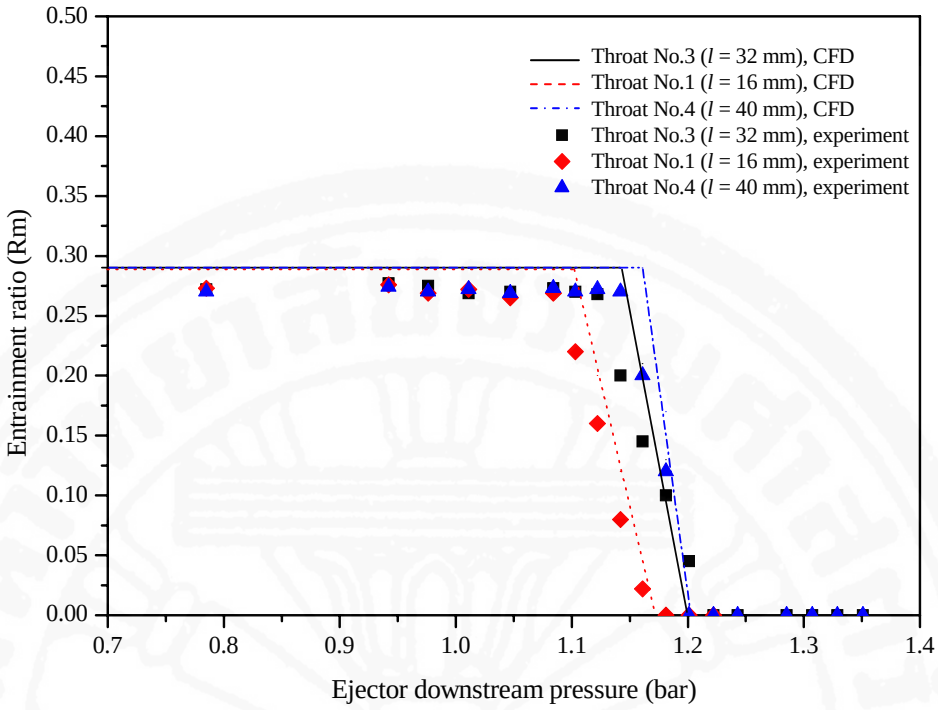

Figure 5.11 Validation of entrainment ratio, effect of throat length.

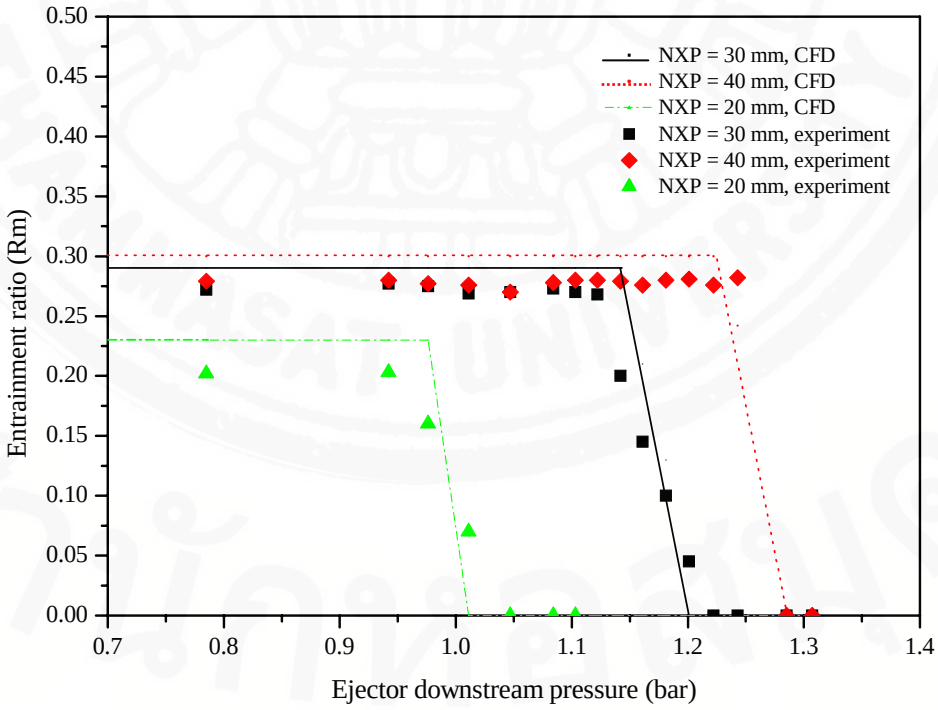

Figure 5.12 Validation of entrainment ratio, effect of nozzle exit position.

The comparison between the CFD analysis and the experimental results of the ejector's performance at the critical point and critical back pressure of the experiment R141b ejector are also illustrated in Table B.2. Figure 5.13 shows the comparison between the CFD and the experimental results of the entrainment ratio in the choked and the unchoked flow region. At the unchoked flow region, Figure 5.13 b), the distribution of the error in predicted values of the entrainment ratio to the experimental ones is wider than the ones at the choked flow region, Figure 5.13 a). Possible reasons for this error may come from, firstly, the difficulty of calibrating the absolute pressure transducer. In the unchoked flow region, the entrainment ratio is subjected to change sensitively to the change of downstream pressure. A slight change in the downstream pressure causes more effect to the entrainment ratio than was found in the choke flow region. Hence, a small error in calibrating the absolute pressure transducer may result in an error in reading the entrainment ratio. Secondly, a very complicated flow at the unchoked flow region, due to shocking behavior, probably gives unexpected results in the experiment.

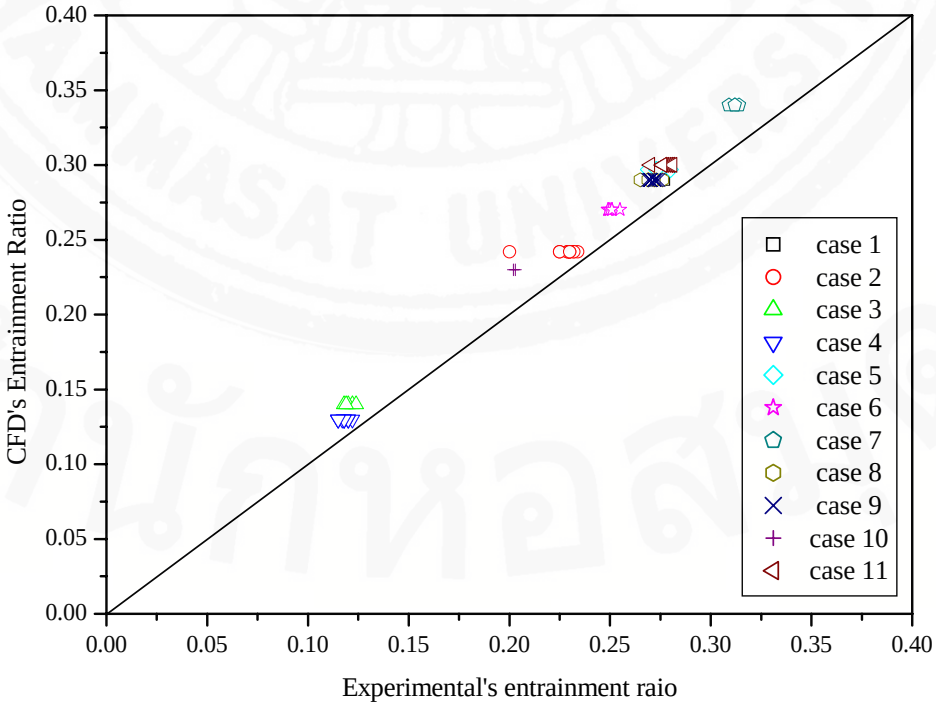

a) Choked flow region

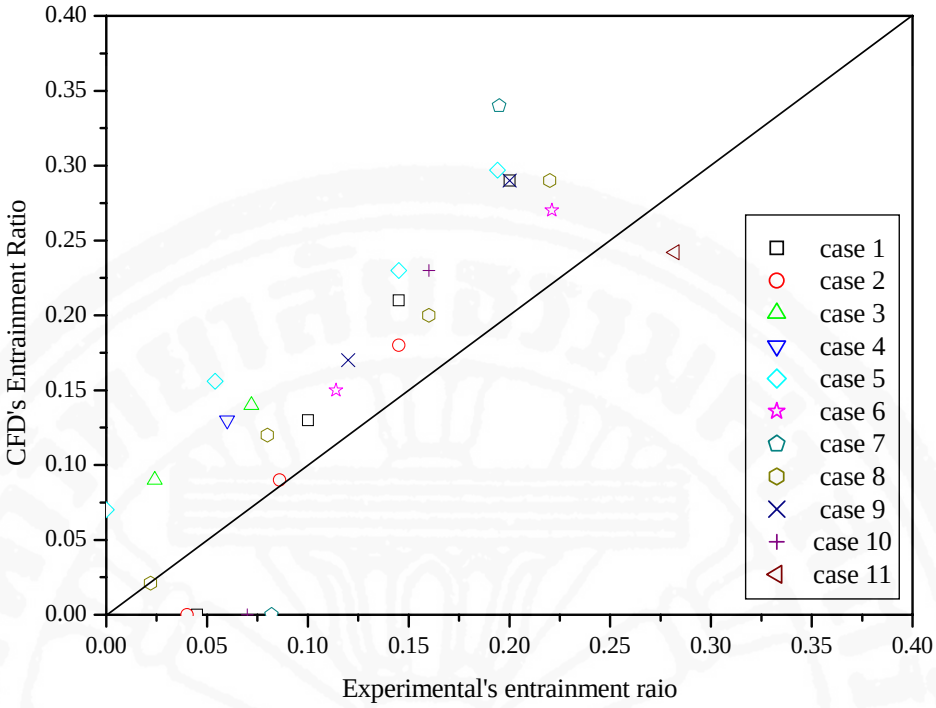

b) Unchoked flow region

Figure 5.13 Comparison between the CFD and the experimental results of the entrainment ratio in the choked flow and the unchoked flow region for various operating conditions and geometries (case 1 to case 11 correspond to the experimental cases in Table B.1).

Comparison between the CFD and the experimental results of the critical back pressure (the highest possible condenser pressure) is shown in Figure 5.14. It is obvious that the overall CFD calculated results agree well with actual values.

Overall, it may be concluded that, the comparison demonstrates the proficiency of the CFD model in predicting an accurate performance for both entrainment ratio and critical back pressure of a typical designed ejector. Average errors of the predicted entrainment ratio and the critical back pressure were both found to be less than 9% and 2%, respectively.

.

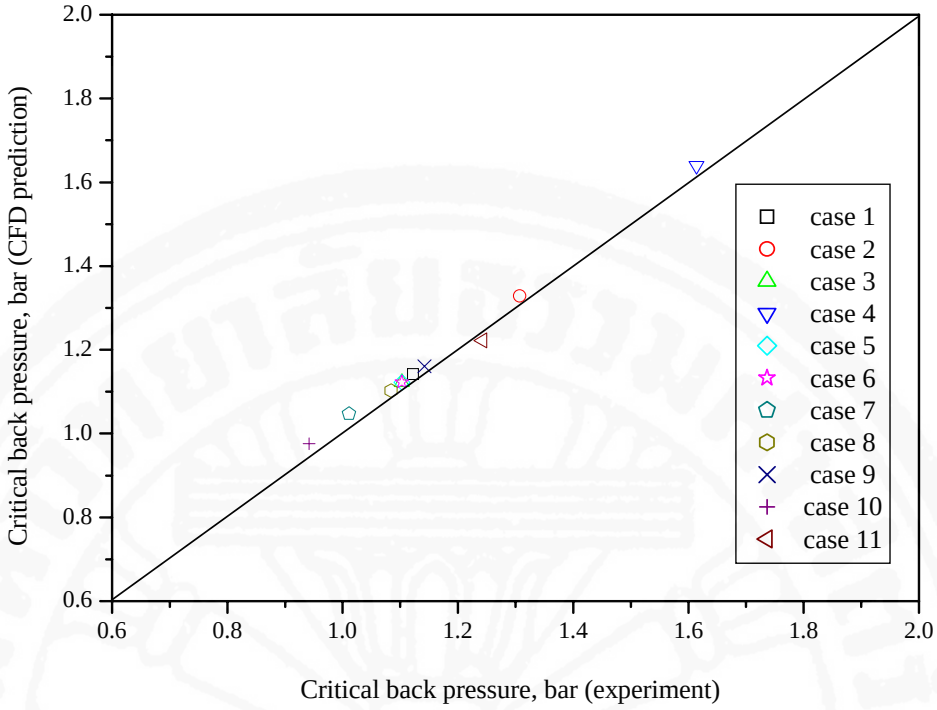

Figure 5.14 Comparison between the CFD and the experimental results of the critical back pressure for various operating conditions and geometries (case 1 to case 11 correspond to the experimental cases in Table B.1)**.**

5.4 Conclusions

This chapter demonstrates the validation of the CFD results and the experimental data obtained from the constructed experimental R141b ejector refrigerator. Three types of the following information were used to validate the simulated model:

- The primary fluid's mass flow rate
- The static pressure distribution at the wall of the ejector
- The entrainment ratio including its critical back pressure

It was verified that the CFD method is an efficient tool to predict the entrainment ratio and critical back pressure of the ejector. The tabulated ejector performances from the experiment and the calculations show the accuracy of the model. Even though no correction factors were added as was done in one-dimensional theories, it was found that

the CFD method provides reliable results compared to the actual values from the experiment. Unlike one-dimensional theories, a constant mass flow which is a typical characteristic of an ejector was shown. Even though the errors of calculations were found to be quite large at some points, they could be clarified.

It can be said that the CFD study in this research was just one of the very first studies in the field of the ejector in refrigeration application. In order to utilize this method more efficiently, further studies are needed. From the study, it was shown that the constructed CFD model may not represent the experiment ejector perfectly; therefore, some improvements on the model setup and the calculation domain are needed. For instance, the real gas equations should be applied as the properties of the working fluid rather than using the perfect gas assumption. Moreover, the heat transfer function at the wall surfaces, that allows not only the investigation of heat transfer, but also of condensation during the process, should be turned on so that the model could be more realistic.

After the achievement in validating the simulated results with the experimental values as presented in this chapter, the flow and mixing process within the R141b ejector is explained utilizing other useful information available from the simulated solutions.